Wideband sound absorption of a double-layer microperforated panel with inhomogeneous perforation

Ali I. Mosa [a,b], A. Putra [c,*], R. Ramlan [c], Al-Ameri Esraa [a]

[a] Fakulti Kejuruteraan Mekanikal, Universiti Teknikal Malaysia Melaka, Hang Tuah Jaya, 76100 Durian Tunggal, Melaka, Malaysia
[b] Mechanical Engineering Department, College of Engineering, University of Baghdad, Jadriyah – Baghdad, Iraq
[c] Centre for Advanced Research on Energy, Universiti Teknikal Malaysia Melaka, Hang Tuah Jaya, 76100 Durian Tunggal, Melaka, Malaysia

ARTICLE INFO

ABSTRACT

Micro-perforated panel (MPP) absorber is increasingly gaining popularity as an alternative sound absorber in buildings compared to the well-known synthetic porous materials. A single MPP has a typical feature of a Helmholtz resonator with a high amplitude of absorption but a narrow absorption frequency bandwidth. To improve the bandwidth, a single MPP can be cascaded with another single MPP to form a double-layer MPP. This paper proposes the introduction of inhomogeneous perforation in the double-layer MPP system (DL-iMPP) to enhance the absorption bandwidth of a double-layer MPP. Mathematical models are proposed using the equivalent electrical circuit model and are validated with experiments with good agreement. It is revealed that the DL-iMPP produces a wider half-absorption bandwidth compared to the conventional homogeneous double-layer MPP. The absorption bandwidth to higher frequencies can be effectively controlled by reducing the air cavity between the iMPPs and to the lower frequencies by increasing the back cavity depth at the second layer.

© 2019 Elsevier Ltd. All rights reserved.

1. Introduction

A micro-perforated panel (MPP) has been introduced as an alternative absorber to the traditional fibrous and porous absorbers. The MPP absorber is made of a thin panel containing a set of tiny holes with less than 1 mm in diameter [1,2]. The MPP is then placed in front of a rigid wall separated by an air cavity to generate a sound absorption mechanism similar to a Helmholtz resonator when it is impinged by a sound field. The frequency of its absorption peak can be controlled by adjusting the hole diameter, the perforation ratio, thickness of the panel, or the back air cavity. As the MPP can be made of a solid panel, its optical feature adds aesthetic value and provides attractive appearances in room interior.

Numerous studies have been proposed to improve the absorption frequency bandwidth of the MPP. The studies presented modifications of the conventional single layer of MPP which include installation a honeycomb structure at the back of the MPP [3,4], construction of holes with tapered geometry [5,6], reduction of hole diameter into ultra-micro size [7], addition of parallel-extended tubes [8,9] and introduction of inhomogeneous perforation [10].

The performance of a single MPP can also be improved by adding layers of MPP to form a multi-layered MPP system [1,11–14]. The multi-layered MPP produces additional resonant peaks, which enhances the absorption frequency bandwidth. The peak frequencies can be controlled by adjusting the air cavity between the MPPs and the back air cavity, which controls the bandwidth of the half-power absorption (absorption coefficient is more than 0.5). Most recently, Qian et al. [15] proposed a double-layer MPP by modifying the back cavity into sub-cavities with different depths. It was demonstrated that absorption coefficient of almost unity can be achieved in the frequency range of 400 Hz to 2 kHz by controlling the hole diameter, the perforation ratio, and the cavity depth. The same performance can also be achieved within frequency range of 1.5–6.5 kHz for other combinations of parameters. These two sets of double-series MPPs can then be combined into a parallel arrangement to form an MPP system with a wider absorption bandwidth.

This paper proposes a double-layer MPP model where each layer of the single MPP comprises of inhomogeneous perforation (denoted here as DL-iMPP). It combines the benefit of a double-layer MPP and inhomogeneous perforation to provide a further improvement on the absorption frequency bandwidth, as demonstrated in [10,11]. The double-layer MPP proposed here is developed with uniform cavities for ease of construction. Also, it is

* Corresponding author.
E-mail address: azma.putra@utem.edu.my (A. Putra).

perforated with conventional sub-millimetric holes to reduce the dependency on the sophisticated technology to produce holes with the accuracy up to 0.01 mm as presented in [15,16].

The mathematical model used here employs the equivalent electrical circuit model (ECM) to represent the acoustic impedance of the DL-iMPP system. The ECM was used in various works related to MPP, starting from the pioneering work by Maa [1] to the subsequent works in an attempt to improve the absorption bandwidth of the MPP absorbers. The ECM has been demonstrated to predict the absorption coefficient quite accurately [10,15,17–19]. However, the application of ECM is limited for evenly distributed holes in the panel [17]. In addition, it cannot accurately predict the cavity impedance between MPPs [20], and it ignores the additional fluid mass from neighboring holes which can increase the resonant frequency especially when the distance between holes is relatively small [21].

In this paper, the mathematical model is first proposed for the DL-iMPP model using the ECM and followed by the experimental work to validate the proposed model. Finally, the parametric study is presented discussing the performance of sound absorption of the DL-iMPP for different perforation parameters, different cavity depths between the iMPPs, and also different back cavity depths.

## 2. Governing mathematical model

2.1. Single MPP absorber

The basic structure and the theory of the micro-perforated panel (MPP) absorber was first proposed by Maa [1,2]. It consists of a single MPP with thickness t and sub-millimetric perforation holes, backed by a rigid wall with an air cavity of depth D. The schematic diagram of this MPP is shown in Fig. 1(a). The specific acoustic impedances of the MPP consist of a resistive part (corresponds to the viscous effect between the air and inner surface of the hole) and an imaginary part (corresponds to the inertial motion of air in the hole) given by

$$Z_{\text{MPP}} = Z_{\text{resistance}} + Z_{\text{reactance}} = r + j\omega m \tag{1}$$

with

$$r = \frac{32\eta t}{\rho c d^2 p}\left(\sqrt{1 + \frac{x^2}{32}} + \frac{xd\sqrt{2}}{8t}\right) \tag{2}$$

$$m = \frac{t}{pc}\left(1 + \left(9 + \frac{x^2}{2}\right)^{-1/2} + \frac{0.85d}{t}\right) \tag{3}$$
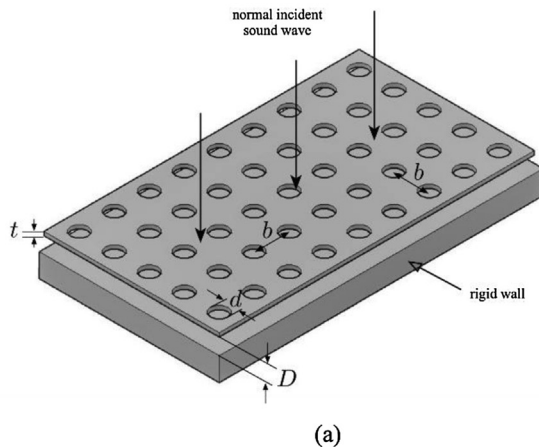
where $x = d/2\sqrt{\omega\rho/\eta}$, p is the perforation ratio $= (\pi/4) * (d/b)^2$ [1], d is the diameter of the holes, b is the distance between holes centers, $\rho = 1.2$ kg/m^3 is the density of air, $c = 344$ m/s is the speed of sound, ω is the angular frequency (in radian per second) and $\eta = 1.84 \times 10^{-5}$ Pa.s is the viscosity of air.

The impedance of the air cavity, D is given by

$$Z_D = -j\cot\left(\frac{\omega D}{c}\right) \tag{4}$$

Note that all the impedances in Eqs. (1)–(4) have been normalized by the impedance of air, ρc. The equivalent electric circuit model (ECM) for the acoustic impedance of the MPP is shown in Fig. 1(b). The total acoustic impedance is thus given by

$$Z_{\text{total}} = Z_{\text{MPP}} + Z_D \tag{5}$$

The sound absorption coefficient is calculated by

$$\alpha = \frac{4Re\{Z_{\text{total}}\}}{[1 + Re\{Z_{\text{total}}\}]^2 + Im\{Z_{\text{total}}\}^2} \tag{6}$$

The normalization of the impedance in Eqs. (1)–(3) with the perforation ratio, p implies that the hole impedance is evenly distributed across the plate surface [22]. This assumption is valid for the case where hole locations are also evenly distributed in the plate, and the distance between holes is much smaller than half-wavelength of the impinging sound. In his model, Maa [1] might have indirectly considered the effect of the hole distance on the impedance. A more detailed study, however, can be referred to the work in [23], where the hole distance b is varied, while the perforation ratio p is maintained (unevenly distributed holes). The end correction of the hole impedance is then modified using the Fok's function, given by the ratio between then perforation ratio and the hole distance, p/b. The study reveals that as the hole distance b decreases, the peak frequency of absorption coefficient shifts to lower frequency. This is due to the additional mass from the nearby holes at the vicinity of hole edge affecting the resonant frequency of the MPP. The model proposed in this paper assumes the holes are located far apart and this hole interaction effect is therefore not taken into account.

2.2. Double-layer inhomogeneous MPP absorber

The sound absorption performance of MPP, especially towards the low-frequency bandwidth can be improved by adding another layer of MPP to form a double-layer MPP absorber [11]. In this study, a similar double-layer arrangement MPP model is
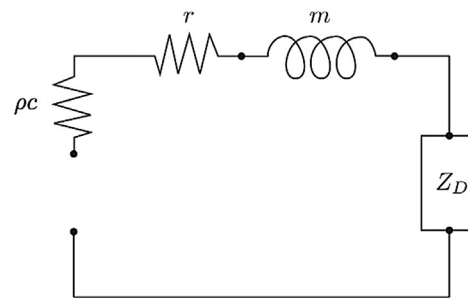
Fig. 1. Schematic diagram of uniform-size single layer MPP absorber and its equivalent electro-acoustic circuit.

proposed, but now each MPP is equipped with inhomogeneous perforation (iMPP). This combination is to integrate the advantages of a double-layer MPP and the inhomogeneous perforation in a single system (DL-iMPP) which can widen the absorption frequency bandwidth. The model structure is created by arranging two MPPs in series. Each panel has two sub-MPPs having a different hole diameter and perforation ratio to create an inhomogeneous pattern, as shown in Fig. 2. The first layer of the inhomogeneous MPP is denoted as $iMPP_1$, and the second layer is $iMPP_2$.

For the second layer $iMPP_2$, two cases are discussed in this paper regarding the back air cavity of the $iMPP_2$:

(i) The back cavity has a partition separating the cavity. Each sub-MPP has its own, isolated back cavity.
(ii) The back cavity has no partition, where both sub-MPPs share the same back cavity.

2.2.1. Back air cavity with partition

The ECM where the back cavity of $iMPP_2$ is separated by a partition is shown in Fig. 3. Similar studies of using ECM to model MPPs with separated cavity are also presented in [17,24] which show an accurate prediction and much simpler calculation compared to other models.

The two iMPPs are assumed to be acoustically rigid to disregard the vibration effect on the panel under acoustic loading. The impinging sound wave is at normal incidence. The specific acoustic impedance for $iMPP_1$ is

$$\frac{1}{Z_{iMPP_1}} = \frac{1}{Z_{MPP_{sub1}}} + \frac{1}{Z_{MPP_{sub2}}} \tag{7}$$

where the impedance of each sub-MPP, $Z_{MPP_{sub}}$ is calculated using Eq. (1).

The next step is to solve the impedance for the second layer iMPP. The second layer of the iMPP consists of two sub-MPPs backed by the same depth of air cavity, D_2. The cavity is separated by a partition forming a parallel arrangement between the corresponding sub-MPPs. The specific acoustic impedance of the second layer including each corresponding back cavity therefore consists of

$$Z_3 = Z_{MPP_{sub3}} + Z_{D_2} \tag{8}$$

$$Z_4 = Z_{MPP_{sub4}} + Z_{D_2} \tag{9}$$

and its equivalent impedance is therefore given by

$$\frac{1}{Z_{3,4}} = \frac{a_3}{Z_3} + \frac{a_4}{Z_4} \tag{10}$$

where $a_3 = A_3/A_{iMPP_2}$ and $a_4 = A_4/A_{iMPP_2}$, are the area ratio for MPP_{sub3} and MPP_{sub4}, respectively. Fig. 4 shows the ECM where the impedance of $Z_{3,4}$ is parallel with the impedance of the air cavity between the iMPPs, i.e. Z_{D_1}.

From Fig. 4, the total impedance is thus given by

$$Z_{DL\text{-}iMPP} = Z_{iMPP_1} + \left[\frac{1}{Z_{3,4}} + \frac{1}{Z_{D1}}\right]^{-1} \tag{11}$$

Note that the impedance of the cavity between the iMPPs, Z_{D_1} (calculated using Eq. (4)) is approximated here to be the same as the impedance by the air cavity backed by a rigid wall [1,24]. The sound absorption coefficient can be calculated by using Eq. (6).

2.2.2. Back air cavity without partition

In this model, the back air cavity of the second layer of $iMPP_2$ is of uniform depth, and without a separated partition. The ECM is shown in Fig. 5. The specific acoustic impedance of the second layer, $iMPP_2$ is given by

$$\frac{1}{Z_{iMPP_2}} = \frac{1}{Z_{MPP_{sub3}}} + \frac{1}{Z_{MPP_{sub4}}} \tag{12}$$

And the total impedance of the second layer including its backed cavity is thus given by

$$Z_{3,4} = Z_{iMPP_2} + Z_{D_2} \tag{13}$$

The simplified ECM is the same as in Fig. 4. The total impedance can thus be calculated using Eq. (11) and the absorption coefficient can be obtained from Eq. (6).

3. Model validation

3.1. Experimental setup

For the experiment, all the iMPP samples were made of PVC-U material with thickness of 1 mm and 2 mm. The iMPPs were arranged in a cylindrical case made of the same material with an outer diameter of 33 mm to fit in the impedance tube, as shown in Fig. 6. The perforation parameters used are based on the findings in [10], where the two sub-MPPs at each iMPP layer were constructed with a large difference in hole diameter and perforation ratio between the corresponding sub-MPPs to produce a wide frequency bandwidth of absorption. The perforation ratio, the hole diameter, and the thickness of each iMPP are shown in Table 1. Fig. 7 shows the cross-section view of the arrangement of the iMPP samples in the cylindrical casing.

Measurement of the absorption coefficient was performed in an impedance tube based on the transfer function method according to the ISO 10534-2 [25]. The tube has an inner diameter of 33 mm and an outer diameter of 55 mm. The distance between the first microphone and the loudspeaker is 212.5 mm, the distance between the two microphones is 22.5 mm, and the distance from the second microphone to the front of the sample is 85.5 mm. This setup arrangement gives the lowest valid frequency of around
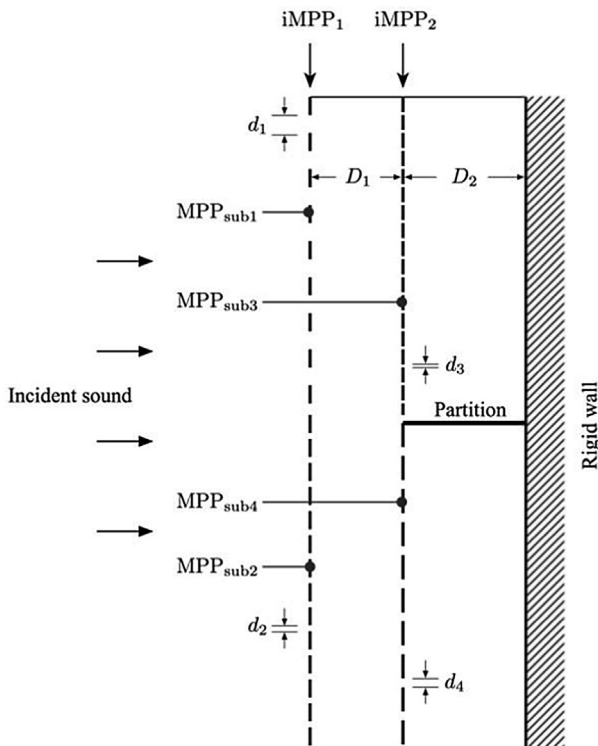

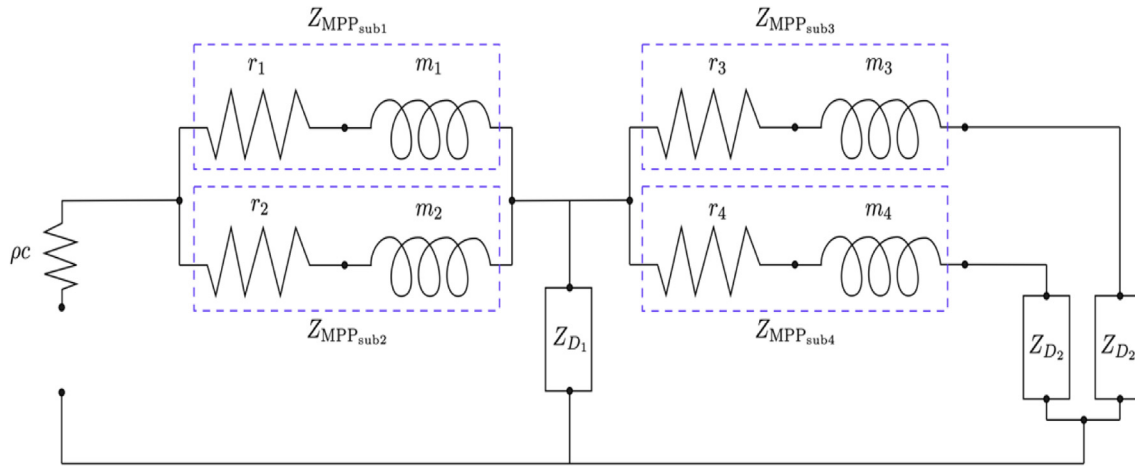**Fig. 2.** Schematic diagram of the double layer inhomogeneous MPP absorber.

Fig. 3. The electrical equivalent circuit model for the case where the back cavity of the iMPP$_2$ is separated by a partition.
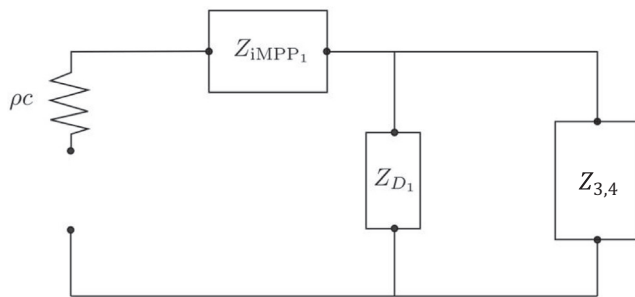

Fig. 4. The simplified electrical equivalent circuit model of Fig. 3.

500 Hz [25]. Two ½-in pre-polarised free-field acoustic microphones (GRAS 40AE) with ½-in CCP pre-amplifier (GRAS 26CA) were used. The microphone's sensitivity was calibrated using Brüel & Kjær sound calibrator type 4231 at 114 dB level and 1 kHz. The schematic diagram of the measurement setup is shown in Fig. 8.

3.2. Experimental results and validation

The comparison between the predicted and the measured normal absorption coefficient of the DL-iMPP is shown in Fig. 9 for the case where the cavity has a partition. The results are presented in the frequency range of 500 Hz to 3 kHz to focus only at the area of high absorption.

It can be observed that the predicted and the measured results have a good agreement. Some fluctuations of peaks can be seen in the measured results, but in general, the trend of the absorption coefficient between the two results is almost the same. The fluctuations within the frequency range of 1–2.5 kHz, shown in Fig. 9(a) and (b), are maybe due to the vibration of the thin partition in the second layer back air cavity, which may also cause an unstable sound field in the cavity.

Based on the measured results, the half-absorption bandwidth, i.e., where the absorption coefficient has a value of at least 0.5, extends from 500 Hz to 1.70 kHz in Fig. 9(a), 500 Hz to 2.65 kHz in Fig. 9(b) and from 500 Hz to 2.6 kHz in Fig. 9(c).

In Fig. 10, the results are presented for the DL-iMPP without the partition in the second layer cavity. The measurement data, in general, has the same trend with the proposed model. In Fig. 10(a) and (b), particularly, it can be seen that the fluctuations are now much less compared to those in Fig. 9. The half-absorption bandwidth extends from 500 Hz to 1.6 kHz in Fig. 10(a), 500 Hz to 2.7 kHz in Fig. 10(b), and 500 Hz to 2.75 kHz in Fig. 10(c). However it can be observed here that the first peak frequency from the prediction over-estimates the measured peak frequency. As the first peak strongly corresponds to the back cavity depth at the second layer (see later in Section 4.3), this disagreement may be due to the
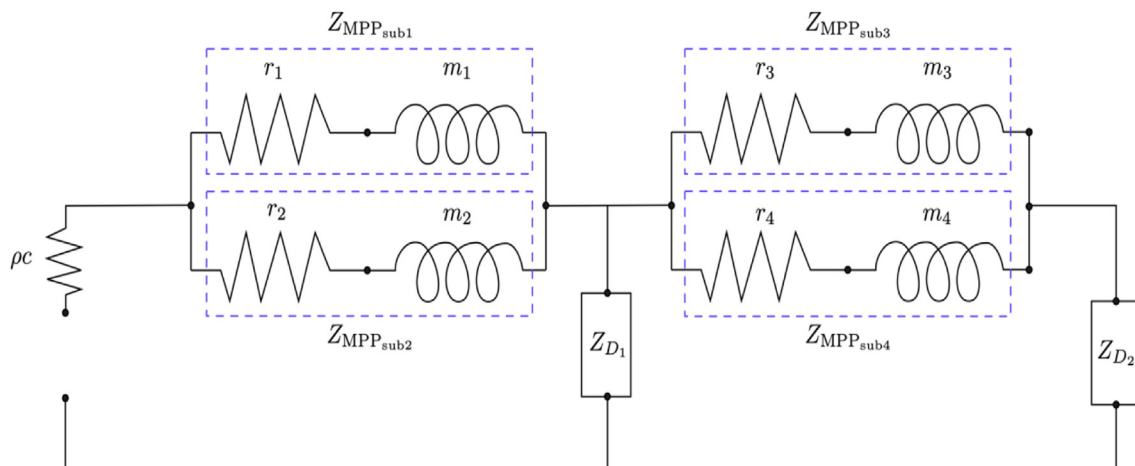

Fig. 5. The electrical equivalent circuit model for the case where the back cavity of the iMPP$_2$ is not separated by a partition.
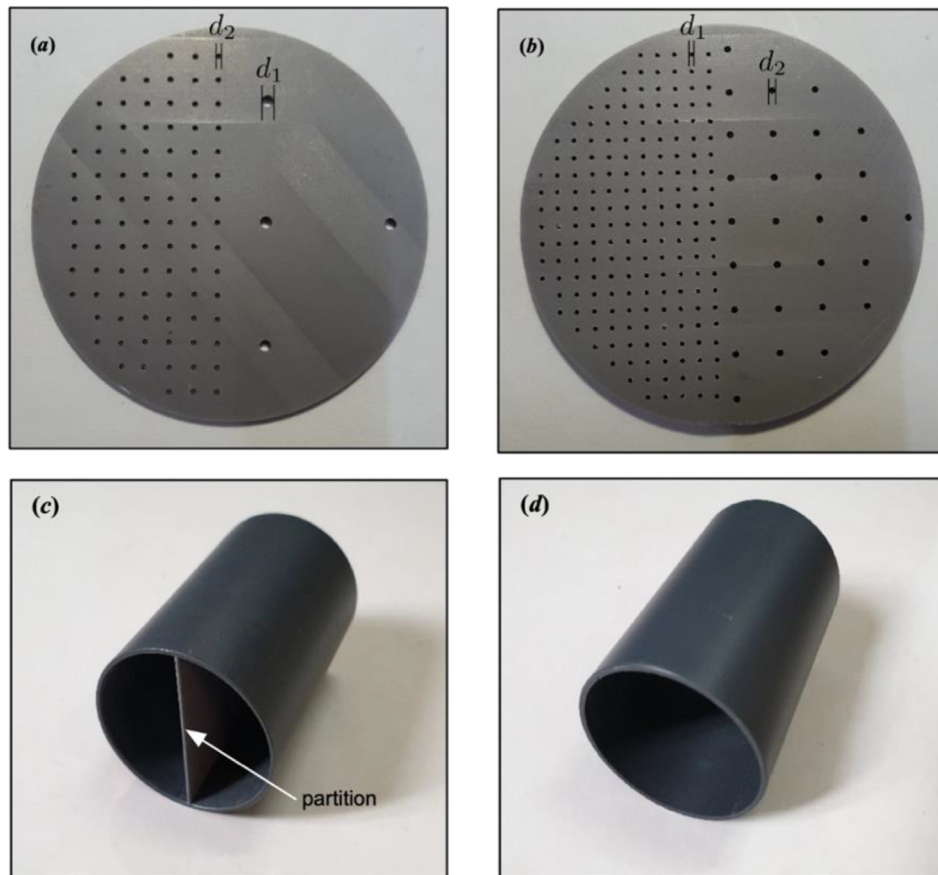
Fig. 6. The iMPPs samples and the cylindrical cases used in experiment: (a) iMPP$_1$, (b) iMPP$_2$, (c) casing with a partition and (d) casing without a partition.

Table 1
Perforation parameters of the test iMPPs samples.

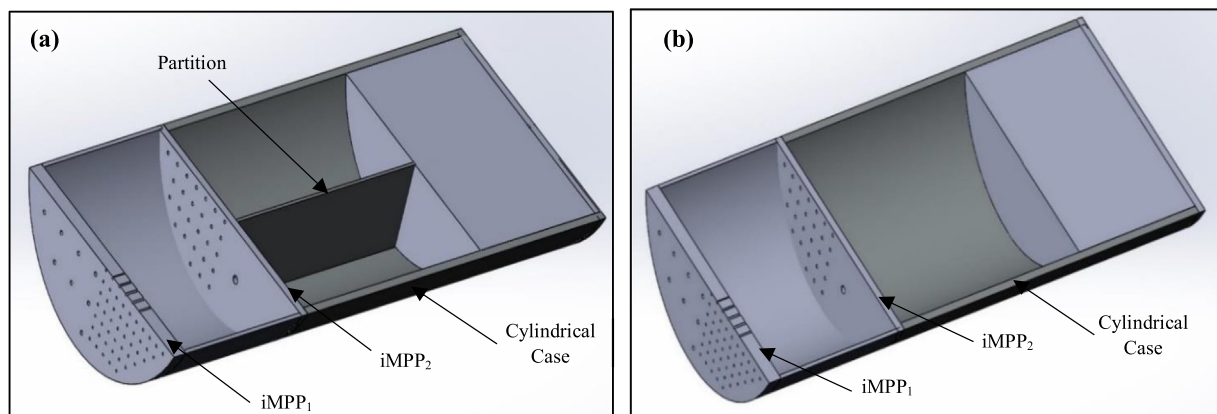| Sample	Parameters				
	d_1 (mm)	d_2 (mm)	p_1 (%)	p_2 (%)	t (mm)
iMPP$_1$	0.9	0.4	0.6	3.0	1
iMPP$_2$	0.3	0.5	3.5	1.5	2

Fig. 7. Cross-section views of the DL-iMPP samples: (a) with a partition separating the back cavity of the iMPP$_2$ and (b) without the cavity partition.
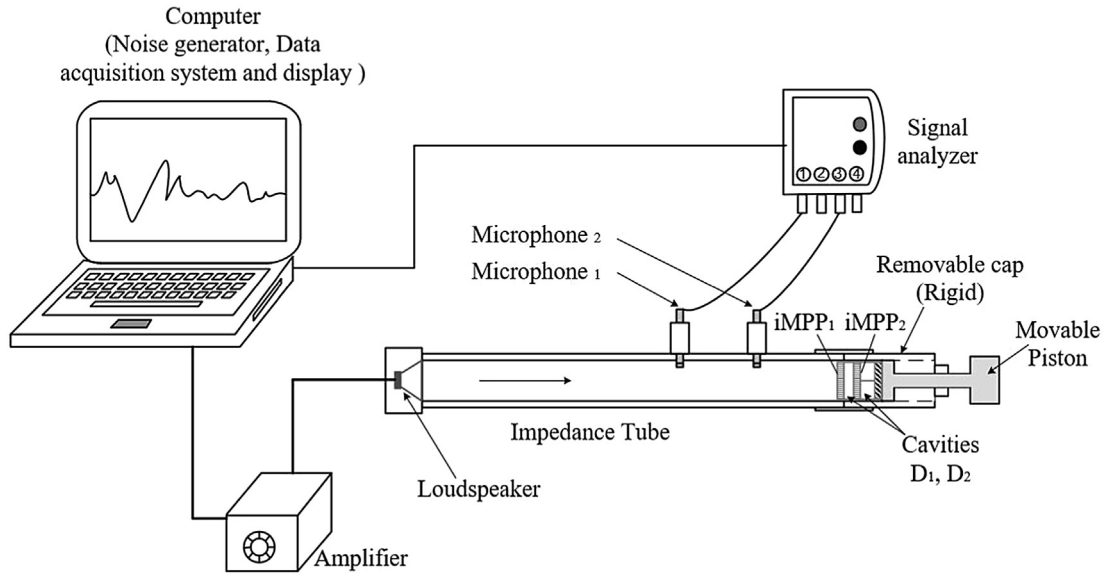
Fig. 8. Experimental setup for the measurement of absorption coefficient of the DL-iMPP absorber.

Fig. 9. Comparison between the predicted and measured absorption coefficients of the DL-iMPP system (with partition): (a) D_1 = 10 mm, D_2 = 22 mm; (b) D_1 = 20 mm, D_2 = 22 mm; (c) D_1 = 20 mm, D_2 = 32 mm.
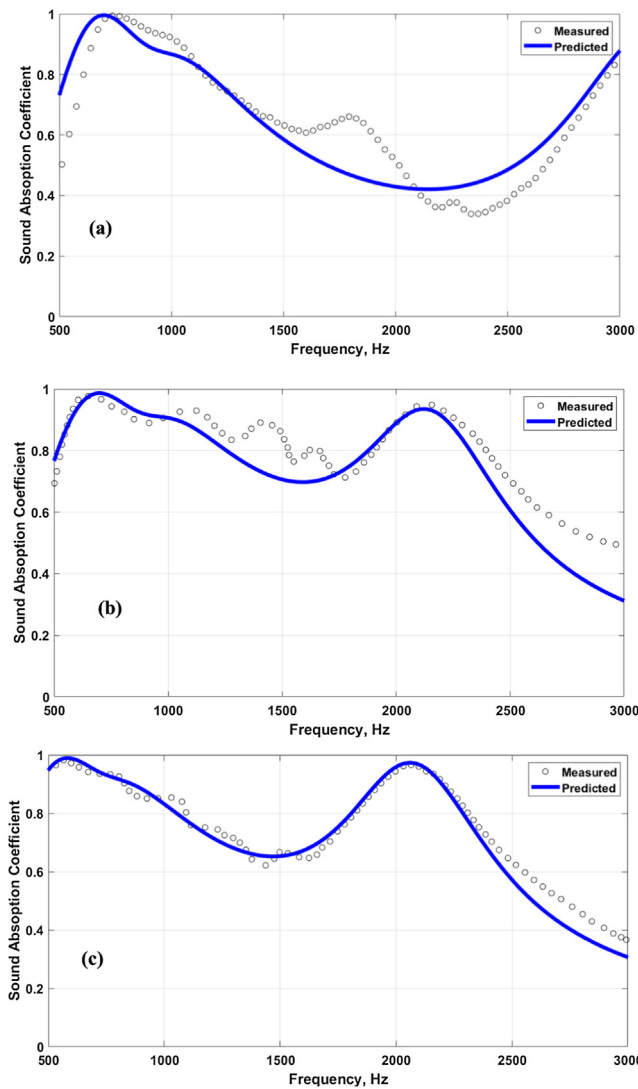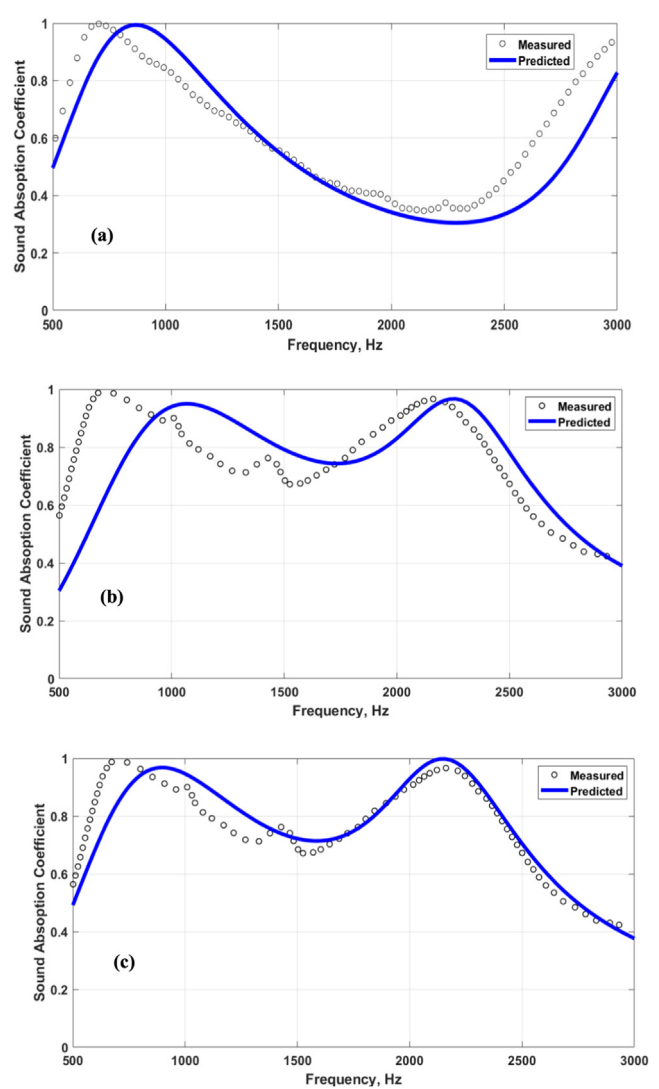
Fig. 10. Comparison between the predicted and measured absorption coefficients of the DL-iMPP system (without partition): (a) D_1 = 10 mm, D_2 = 22 mm; (b) D_1 = 20 mm, D_2 = 22 mm; (c) D_1 = 20 mm, D_2 = 32 mm.
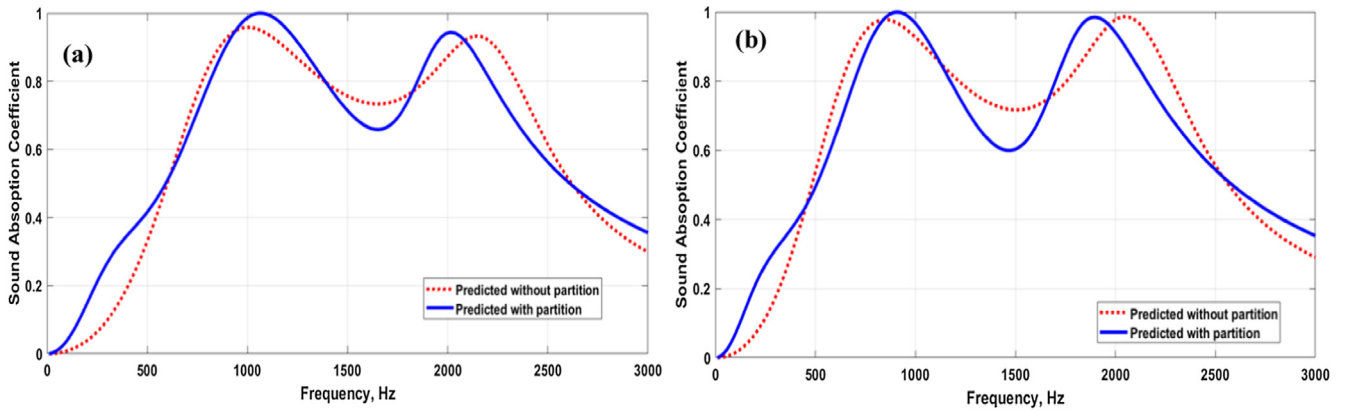
Fig. 11. Comparison between absorption coefficients of the DL-iMPP with and without backed cavity partition: iMPP$_1$: $t_1 = 1$ mm, $d_1 = 0.6$ mm, $d_2 = 0.3$ mm, $p_1 = 0.6\%$, $p_2 = 3.0\%$ and iMPP$_2$: $t_2 = 2$ mm, $d_3 = 0.3$ mm, $d_4 = 0.5$ mm, $p_3 = 4.0\%$, $p_4 = 0.2\%$; (a) D$_1 = 20$ mm, D$_2 = 22$ mm, (b) D$_1 = 20$ mm, D$_2 = 32$ mm.

Fig. 12. Comparison between absorption coefficients of the DL-iMPP with and without backed cavity partition: iMPP$_1$: $t_1 = 1$ mm, $d_1 = 0.9$ mm, $d_2 = 0.4$ mm, $p_1 = 0.6\%$, $p_2 = 3.0\%$ and iMPP$_2$: $t_2 = 2$ mm, $d_3 = 0.5$ mm, $d_4 = 0.3$ mm, $p_3 = 1.0\%$, $p_4 = 3.5\%$; (a) D$_1 = 20$ mm, D$_2 = 22$ mm, (b) D$_1 = 20$ mm, D$_2 = 32$ mm.
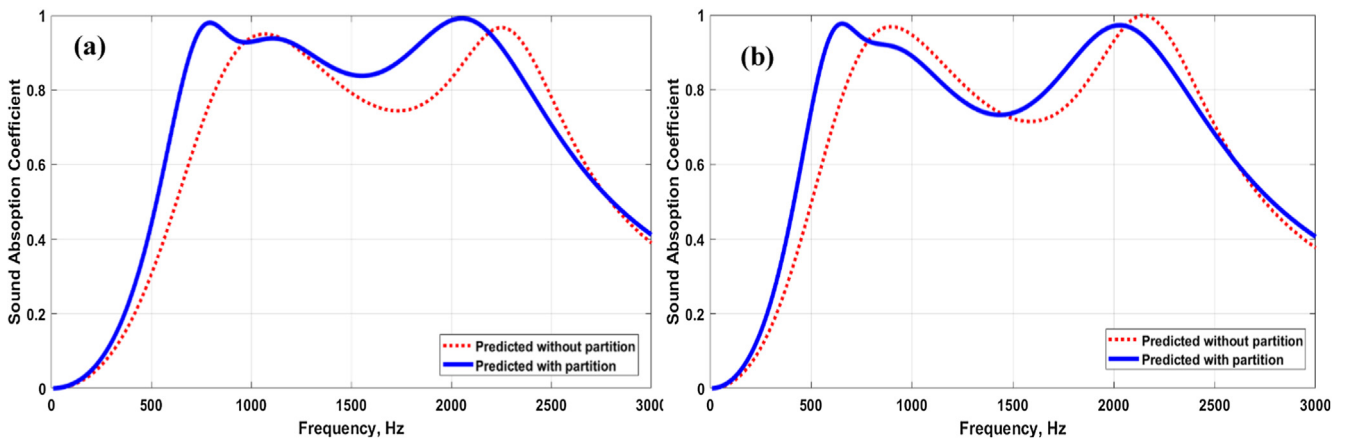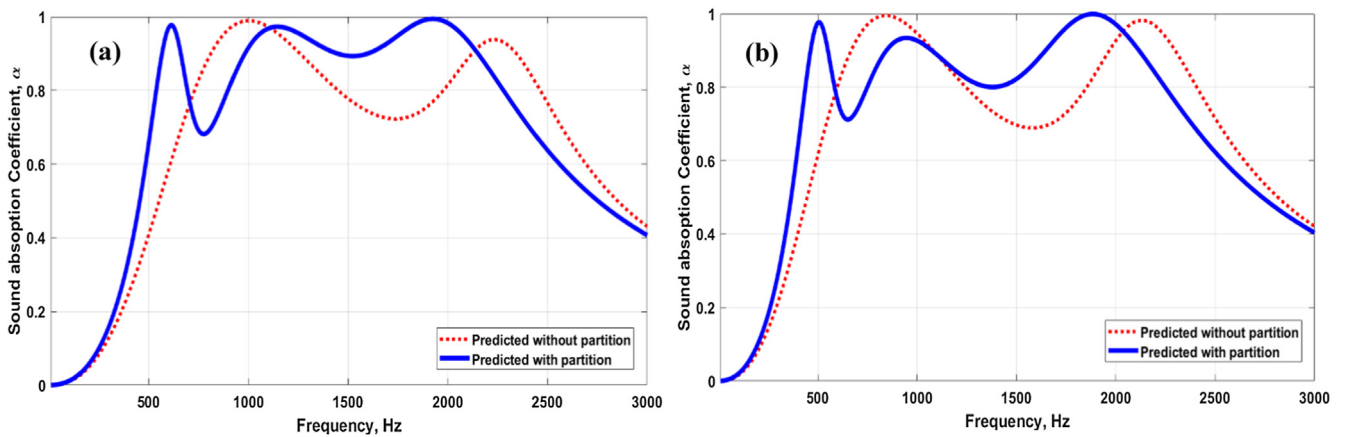

Fig. 13. Comparison between absorption coefficients of the DL-iMPP with and without backed cavity partition: iMPP$_1$: $t_1 = 1$ mm, $d_1 = 0.9$ mm, $d_2 = 0.3$ mm, $p_1 = 0.8\%$, $p_2 = 2.5\%$ and iMPP$_2$: $t_2 = 2$ mm, $d_3 = 0.3$ mm, $d_4 = 0.8$ mm, $p_3 = 4.0\%$, $p_4 = 1.0\%$; (a) D$_1 = 20$ mm, D$_2 = 22$ mm, (b) D$_1 = 20$ mm, D$_2 = 32$ mm.

assumption made in the ECM, where the impedance of the back air cavity is modelled as a shared impedance to both sub-MPPs (see Fig. 5), while in reality, each sub-MPP at certain degree may still act independently with the back air cavity, similar to the case for the cavity with partition.

The next section discusses the comparison of sound absorption of the double-iMPP system with and without the partition in the back cavity for other MPP parameters calculated from the proposed models.

4. Model simulation

4.1. DL-iMPP with and without the cavity partition

Figs. 11–13 plot the absorption coefficient of DL-iMPP, with and without the partition at the second layer cavity, for different perforation parameters and cavity depths. It can be seen that introducing the partition slightly shifts absorption peaks to the lower frequency. The degree of the frequency shift depends on

Table 2
Parameters of double-layer homogeneous MPP (DL-MPP) and double layer inhomogeneous MPP (DL-iMPP).

(a)

Model	MPP layer 1					MPP layer 2				
	d_1 (mm)	d_2 (mm)	p_1 (%)	p_2 (%)	t (mm)	d_1 (mm)	d_2 (mm)	p_1 (%)	p_2 (%)	t (mm)
DL-MPP 1	0.9		0.16		1.0	0.3		4.0		2.0
DL-MPP 2	0.3		1.0		1.0	0.5		3.2		1.0
DL-iMPP	0.9	0.3	0.16	4.0	2.0	0.5	0.3	1.0	3.2	1.0

(b)

Model	MPP layer 1					MPP layer 2				
	d_1 (mm)	d_2 (mm)	p_1 (%)	p_2 (%)	t (mm)	d_1 (mm)	d_2 (mm)	p_1 (%)	p_2 (%)	t (mm)
DL-MPP 1	0.9		3.2		0.5	0.7		3.2		0.5
DL-MPP 2	0.2		1.5		1.0	0.3		1.5		1.0
DL-iMPP	0.9	0.3	0.6	1.5	0.5	0.2	0.7	3.2	1.0	1.0

(c)

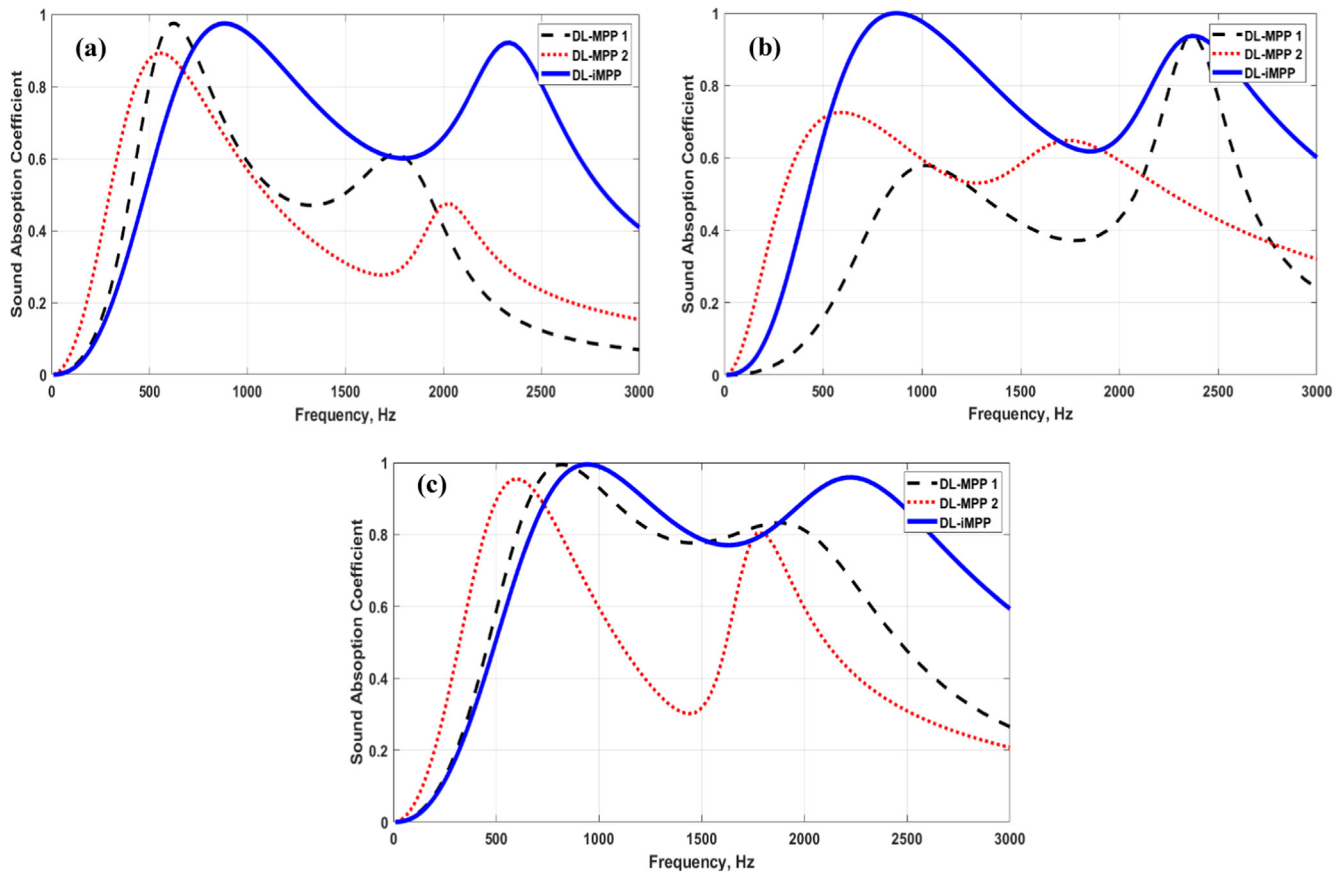| Model	MPP layer 1					MPP layer 2				
	d_1 (mm)	d_2 (mm)	p_1 (%)	p_2 (%)	t (mm)	d_1 (mm)	d_2 (mm)	p_1 (%)	p_2 (%)	t (mm)
DL-MPP 1	0.8		3.5		0.5	0.3		0.8		0.5
DL-MPP 2	0.3		2.5		2.0	0.8		3.5		2.0
DL-iMPP	0.8	0.3	0.6	2.5	0.5	0.3	0.8	3.5	0.8	2.0

Fig. 14. Comparison of absorption coefficients between inhomogeneous DL-iMPP and homogeneous DL-MPP (cavity depth: D_1 = 20 mm, D_2 = 32 mm).

the perforation parameters for each iMPP in the DL-iMPP system.

The distinct peaks for the case of partitioned cavity at 800 Hz in Fig. 12(a) and 600 Hz in Fig. 12(b), and also at 600 Hz at Fig. 13(a) and at 500 Hz in Fig. 13(b) are contributed from the second layer iMPP controlled by the diameter of the holes as highlighted in [10]. The DL-iMPP with the partitioned back cavity can, therefore, be of benefit for sound absorption targeted at a lower frequency. However, as it can also be observed, the difference in half-absorption bandwidth is insignificant for both cases. Moreover, if the finding from the measurement is taken into account, i.e. where the first peak frequency from the measurement appears slightly at the lower frequency than the peak from the prediction, then the difference of absorption coefficient between the two cases (with and without partition) is even smaller. For the subsequent sections, the parametric study is presented only for the DL-iMPP system without the back cavity partition for ease of analysis.
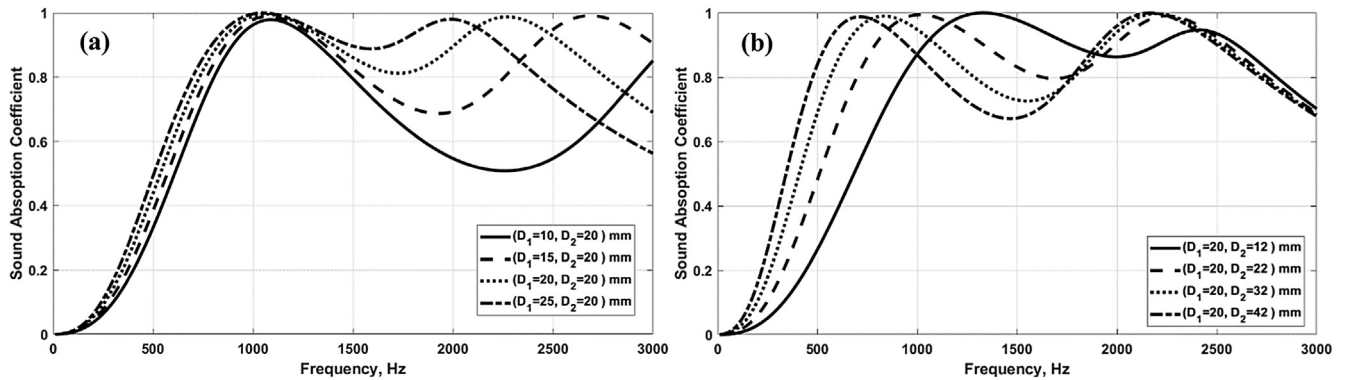
Fig. 15. Absorption coefficients of inhomogeneous DL-iMPP with varying cavity depth; iMPP$_1$: t_1 = 0.5 mm, d_1 = 0.8 mm, d_2 = 0. 2 mm, p_1 = 0.6%, p_2 = 2.0% and iMPP$_2$: t_2 = 2 mm, d_3 = 0.3 mm, d_4 = 0.7 mm, p_3 = 3.5%, p_4 = 0.5%; (a) D_1 varied, D_2 fixed and (b) D_1 fixed, D_2 varied.

4.2. DL-iMPP and DL-MPP

This section discusses the comparison of absorption coefficients between the double-layer MPP with homogeneous perforation (denoted here as DL-MPP) and from the double-layer MPP with inhomogeneous perforation (DL-iMPP). The perforation parameters for both systems are listed in Table 2. For a clear comparison, the hole diameter and the perforation ratio for the DL-iMPP are taken from the parameters of the homogeneous DL-MPP to observe the improvement provided by the DL-iMPP. The cavity depths are the same.

Fig. 14 demonstrates that the DL-iMPP produces a significantly wider absorption bandwidth and larger amplitude of absorption coefficient compared to those from the DL-MPP. Again, the optimum absorption frequency bandwidth and amplitude for the DL-iMPP system can be obtained, provided that each iMPP layer consists of a combination of large hole diameter with a small perforation ratio and small hole diameter with a large perforation ratio. This configuration has been shown in [10] to produce wide absorption bandwidth for a single iMPP.

4.3. Effect of cavity depth

To optimize the advantage of a double-layer system, the cavity depths can be controlled to produce a combination of absorption bandwidth of each layer of the iMPP. Fig. 15 shows that reducing the cavity depth between the two iMPPs improves the frequency bandwidth in the high frequency region (Fig. 15(a)) while increasing the back air cavity (between the second layer iMPP and the rigid wall) improves the bandwidth of the low frequency region (Fig. 15(b)).

The former, however, can be observed to produce greater effect in improving the absorption bandwidth towards the higher frequency region. It can be seen that for D_1 = 15 mm and D_2 = 30 mm in Fig. 15(a), the half-absorption bandwidth (where α > 0.5) can extend from 600 Hz up to 3 kHz and more. However, as the absorption peaks from the corresponding iMPP (in this case at 1 kHz and at 2.75 kHz) become further apart, the dip produced between the two peaks becomes significant. This can be seen for D_1 = 10 mm and D_2 = 20 mm, where the dip at 2.25 kHz has an absorption coefficient of 0.50. The half-absorption bandwidth increases, but this is compromised with the reduction of absorption coefficient level between the two peaks of absorption.

5. Conclusion

Sound absorption performance of a double-layer MPP with inhomogeneous perforation has been presented. The mathematical models have been validated with experimental data with good agreement. The DL-iMPP with a partition in the back cavity is shown to shift the resonant peaks to a lower frequency. However, the improvement of the half-absorption bandwidth compared to the system without the partition is insignificant.

The DL-iMPP has also been demonstrated to produce a wider frequency band of absorption compared to the homogeneous DL-MPP. The results show that the absorption bandwidth in the high frequency region increases with the reduction of the front cavity depth between the two iMPPs. Meanwhile, the absorption bandwidth in the lower frequency region increases with the increase in the back cavity depth at the second layer. However, despite the increase of the absorption bandwidth in the low and high frequency regions, the reduction of the absorption coefficient due to the formation of dip between the two resonant peaks of absorption must be taken into consideration.

The future study can be extended to propose a mathematical model serving as a design guide for constructing the DL-iMPP. The simple model should enable users to directly obtain information of the perforation parameters and the cavity depths based on the target frequency band of interest for sound absorption.

It is also of interest to further investigate the effect of size of the DL-iMPP system relative to the impinging sound wavelength. As the size becomes much larger than the wavelength (high frequency case), the sound may 'see' the impedance of the sub-MPP in the panel individually rather than as a combined impedance of an inhomogeneous perforation. In this case, as highlighted in Ref. [26], the sound absorption amplitude may be lower than that predicted by the proposed model. This could lead to the design consideration for the periodic structure consisting of multiple DL-iMPPs, that the size of each single DL-iMPP must be much smaller than the wavelength of the target maximum absorption frequency. To observe this phenomenon, validation through experiment, especially in the diffuse-field incidence can be performed.

Declaration of Competing Interest

The authors declare that they have no known competing financial interests or personal relationships that could have appeared to influence the work reported in this paper.

Acknowledgement

References

[1] Maa D. Theory and Design of Microperforated panel sound-absorbing constructions. Sci Sinica 1975;18(1):55–71.

[2] Maa D. Microperforated-Panel Wideband Absorbers. Noise Control Eng J 1987;29:77–84.

[3] Liu J, Herrin DW. Enhancing micro-perforated panel attenuation by partitioning the adjoining cavity. Appl Acoust 2010;71(2):120–7.

[4] Sakagami K, Yamashita I, Yairi M, Morimoto M. Effect of a honeycomb on the absorption characteristics of double-leaf microperforated panel (MPP) space sound absorbers. Noise Control Eng J 2011;59:363–71.

[5] Herdtle T, Stuart Bolton J, Kim NN, Alexander JH, Gerdes RW. Transfer impedance of microperforated materials with tapered holes. J Acoust Soc Am 2013;134(6):4752–62.

[6] Qian YJ, Cui K, Liu SM, Li ZB, Kong DY, Sun SM. Numerical study of the acoustic properties of micro-perforated panels with tapered hole. Noise Control Eng J 2014;62(3):152–9.

[7] Qian YJ, Kong DY, Liu SM, Sun SM, Zhao Z. Investigation on micro-perforated panel absorber with ultra-micro perforations. Appl Acoust 2013;74(7):931–5.

[8] Li D, Chang D, Liu B. Enhancing the low frequency sound absorption of a perforated panel by parallel-arranged extended tubes. Appl Acoust 2016;102:126–32.

[9] Li D, Chang D, Liu B. Enhanced low- to mid-frequency sound absorption using parallel-arranged perforated plates with extended tubes and porous material. Appl Acoust 2017;127:316–23.

[10] Mosa AI, Putra A, Ramlan R, Prasetiyo I, Esraa A. Theoretical model of absorption coefficient of an inhomogeneous MPP absorber with multi-cavity depths. Appl Acoust 2019;146:409–19.

[11] Sakagami K, Morimoto M, Koike W. A numerical study of double-leaf microperforated panel absorbers. Appl Acoust 2006;67(7):609–19.

[12] Sakagami K, Nakamori T, Morimoto M, Yairi M. Double-leaf microperforated panel space absorbers: A revised theory and detailed analysis. Appl Acoust 2009;70(5):703–9.

[13] Sakagami K, Yairi M, Morimoto M. Multiple-Leaf Sound Absorbers with Microperforated Panels: An Overview. Acoust Aust 2010;38(2):76–81.

[14] Bravo T, Maury C, Pinhède C. Enhancing sound absorption and transmission through flexible multi-layer micro-perforated structures. J Acoust Soc Am 2013;134(5):3663–73.

[15] Qian YJ, Zhang J, Sun N, Kong DY, Zhang XX. Pilot study on wideband sound absorber obtained by adopting a serial-parallel coupling manner. Appl Acoust 2017;124:48–51.

[16] Qian YJ, Kong DY, Fei JT. A note on the fabrication methods of flexible ultra micro-perforated panels. Appl Acoust 2015;90:138–42.

[17] Carbajo J, Ramis J, Godinho L, Amado-mendes P. Assessment of methods to study the acoustic properties of heterogeneous perforated panel absorbers. Appl Acoust 2018;133:1–7.

[18] Zhao X, Fan X. Enhancing low frequency sound absorption of micro-perforated panel absorbers by using mechanical impedance plates. Appl Acoust 2015;88:123–8.

[19] Okuzono T, Sakagami K. A finite-element formulation for room acoustics simulation with microperforated panel sound absorbing structures: Verification with electro-acoustical equivalent circuit theory and wave theory. Appl Acoust 2015;95:20–6.

[20] Sakagami K, Matsutani K, Morimoto M. Sound absorption of a double-leaf micro-perforated panel with an air-back cavity and a rigid-back wall: Detailed analysis with a Helmholtz-Kirchhoff integral formulation. Appl Acoust 2010;71(5):411–7.

[21] Carbajo J, Ramis J, Godinho L, Amado-Mendes P, Alba J. A finite element model of perforated panel absorbers including viscothermal effects. Appl Acoust 2015;90:1–8.

[22] Putra A, Thompson DJ. Sound radiation from perforated plates. J Sound Vib 2010;329(20):4227–50.

[23] Tayong R. On the holes interaction and heterogeneity distribution effects on the acoustic properties of air-cavity backed perforated plates. Appl Acoust 2013;74(12):1492–8.

[24] Pieren R, Heutschi K. Modelling parallel assemblies of porous materials using the equivalent circuit method. J Acoust Soc Am 2015;137(2):EL131–6.

[25] International Organization for Standardization, ISO 10534-2, Acoustics-Determination of Sound Absorption Coefficient and Impedance in Impedance Tubes, Int. Stand., 2001.

[26] Yairi M, Sakagami K, Takebayashi K, Morimoto M. Excess sound absorption at normal incidence by two microperforated panel absorbers with different impedance. Acoustical Science and Technology 2011;32(5):194–200.